Interacting SQG Vortices and Passive Scalar Transport

Stefan G. Llewellyn Smith and C. K. Taylor

Mechanical & Aerospace Engineering,
University of California San Diego
sgls@ucsd.edu

Abstract

The surface quasi-geostrophic (SQG) equations are a model for low-Rossby number geophysical flows in which the dynamics are governed by potential temperature dynamics on the boundary. The model can be used to explore the effect on transport of the transition from two-dimensional to three-dimensional mesoscale geophysical flows. On an f-plane with linear stratification, we examine the dynamics of SQG vortices and the resulting three-dimensional flow including contributions at first order in Rossby number going beyond the usual QG equation to compute the velocity. While it is simple to obtain the vertical velocity, finding $O(Ro)$ horizontal flow is more involved. The Finite Time Braiding Entropy (FTBE) of Thiffeault & Budisic is used to quantify the chaotic mixing induced by three point vortices. We also consider the exact SQG vortex solution developed by Dritschel (2011) from the limit of a QG ellipsoid of constant potential vorticity. We examine the interaction of two such vortices and the resulting transport.

1 Introduction

At large scales, the ocean can be modeled as a thin body of fluid spread over a rotating sphere. The vertical velocity is weak compared to the horizontal velocity, of order Rossby number $Ro = U/fL$. While the leading-order dynamics give horizontal velocities, transport could be significantly altered by the weak three-dimensional flow.

This work examines transport due to idealized vortex solutions in the SQG model. Transport was studied by Aref and Pomphrey (1980) under the name "chaotic motion" in the simplified case of point vortices in two-dimensional flow. Aref & Pomphrey (1980) found that three interacting vortices would follow regular trajectories, and four vortices could follow chaotic trajectories. Thus, three point vortices that follow periodic paths can produce chaotic flow and transport in the surrounding fluid. In the ocean, mesoscale vortical structures are observed. Here three SQG point vortex solutions are considered and their resulting chaotic mixing is examined.

In order to analyze the quantitative effect of $O(Ro)$ corrections, it is necessary to use an appropriate measure. In chaotic advection, a relevant property is the complexity of the flow, and one of the most convenient measures of global complexity seems to be topological entropy. Topological entropy represents the exponential growth of the number of distinguishable orbits under the repeated iteration of the flow map: the higher the topological entropy, the more chaotic mixing is present. However, this value is difficult to compute given only a velocity field (Newhouse and Pignataro, 1993; Bowen, 1973). Thiffeault & Budišić have recently developed a tool called Braidlab that, among other functions, calculates the Finite Time Braiding Exponent (FTBE), which approximates topological entropy using particle trajectories (Thiffeault and Budišić, 2014; Budišić and Thiffeault, 2015). The benefit of FTBE over the more commonly used Finite Time Lyapunov Exponent (FTLE) (Peacock and Dabiri, 2010) is that FTBE provides a global

measure of complexity as opposed to a local one (Allshouse and Peacock, 2015), allowing us to compare quantitatively the extent of stirring exhibited by different flows and thus explore the parameter space.

The FTBE depends on the number of trajectories and the length of integration time, so here we fix our analysis to include 64 trajectories. As an estimate, the FTBE also varies slightly according to the time step chosen and the initial conditions of the trajectories. To quantify this variation, 13 different sets of 64 trajectories were used to generate a mean FTBE and standard deviation for each flow considered.

2 Point Vortices

The SQG model presented by Held et al. (1995) is derived from the QG equations for three-dimensional flow on a rotating planet, with the hydrostatic and f-plane approximations. These approximations are appropriate for mesoscale flow. In Cartesian geometry with rotation given by the Coriolis parameter, f, the equations are

$$\begin{aligned} Ro\frac{Du}{Dt} - v &= -\phi_x, \\ Ro\frac{Dv}{Dt} + u &= -\phi_y, \\ \theta &= \phi_z, \\ u_x + v_y + Ro\, w_z &= 0, \\ \frac{D\theta}{Dt} + w &= 0. \end{aligned} \tag{1}$$

with the conventional material derivative

$$\frac{D}{Dt} = \frac{\partial}{\partial t} + \mathbf{u}\cdot\nabla,$$

and where the variables (u, v, w) are the velocities in the (x, y, z) directions, respectively; ϕ is the geopotential height; and θ is the buoyancy. The physical constants in the equations of motion are the Coriolis parameter, f, and the buoyancy frequency, N. An expansion in small $Ro \ll 1$ yields at $O(1)$ (Vallis, 2006; Muraki et al., 1999)

$$\Delta\psi = q, \qquad \psi^s_z = \theta^s, \qquad \frac{Dq}{Dt} = 0, \tag{2}$$

where Δ is the three-dimensional Laplacian, q is the potential vorticity, the superscript s indicates that the variable is evaluated at the surface of the domain (conventionally $z = 0$), and the subscript z indicates the z-derivative. The SQG model is (2) with the more restrictive and dynamically consistent condition that $q = 0$ in the interior.

While the 2D Euler system is governed by the specified vorticity, in SQG flow the system is governed instead by the temperature at the surface. Thus, the analogous point vortex flow in SQG is found from the definition

$$\theta^s = \kappa\delta(x - x_0)\delta(y - y_0)\ . \tag{3}$$

The solution to (2) is

$$\psi = -\frac{\kappa}{2\pi}\frac{1}{|\mathbf{x} - \mathbf{x}_0|}, \tag{4}$$

given in Held et al. (1995). Note that, unlike the 2D case, this solution has three-dimensional dependence. For an arbitrary number of vortices with strengths κ_j and positions $\mathbf{x}_j$, i.e.

$$\Delta\psi = 0, \qquad \psi_z^s = \sum_j \kappa_j \delta(x - x_j)\delta(y - y_j), \tag{5}$$

the solution is the linear combination

$$\psi = -\frac{1}{2\pi} \sum_j \frac{\kappa_j}{|\mathbf{x} - \mathbf{x}_j|} \, . \tag{6}$$

The horizontal evolution of a given point vortex is determined by the sum of contributions of every other vortex in the system, given by

$$\begin{pmatrix} \dot{x}_i \\ \dot{y}_i \end{pmatrix} = -\frac{1}{2\pi} \sum_j{}' \frac{\kappa_j}{|\mathbf{x}_i - \mathbf{x}_j|^3} \begin{pmatrix} y_i - y_j \\ -x_i + x_j \end{pmatrix}, \tag{7}$$

where the prime indicates that the self-interaction $i = j$ is ignored.

This system can be solved for any vortex distribution and initial passive particle position. If the resulting trajectories are strobed at every period of vortex motion and the frame is rotated to remove the vortex shifting, Poincaré maps such as those shown in Figure 1 are obtained. These can be compared to the two-dimensional Poincaré maps given in the first figure in Kuznetsov and Zaslavsky (1998).

It can be seen in Figure 1 that, while the dynamics are purely two-dimensional, the flow has vertical dependence. Even when particles follow regular trajectories (a,b,c), the trajectories change with depth. In the case where mixing is exhibited, the barriers of chaotic motion seem to extend as three-dimensional surfaces, and islands are observed at a range of depths.

Because the vortices are of equal strength and we have fixed $L = 1$, the only varying parameter is H. FTBE vs. H is shown in Figure 2. The boundary between the two regimes of vortex motion is indicated with the vertical dotted line, and it seems that for the lower-energy flows the observed mixing is relatively constant, with a minimum seen right at this regime boundary. Then, as the energy of the vortex configuration increases into the two-orbiting-vortices regime, we see FTBE increasing as well. Comparing the SQG case in Figure 2(a) to the classical two-dimensional case in Figure 2(b) shows the same qualitative trends, but the SQG case exhibits a higher levels of mixing than the classical case. Finally, in Figure 2(c) FTBE is calculated at increasing depth, where the plane of vortex motion is $z = 0$. While the vortices still produce mixing at a depth close to the surface, the FTBE falls steeply at depths below approximately $z = -0.25$.

The effect of varying L in the equal strength case is examined in Figure 3. It is clear from these results that changing L will vary the critical depth at which the FTBE drops steeply. Additionally, L affects the scale of the FTBE, where smaller L leads to overall higher FTBE. Small L implies that the vortices are spaced very near one another, resulting in larger velocity magnitudes in the flow between the vortices. It is perhaps not surprising that these higher velocities lead to more efficient mixing.

The small $O(Ro)$ corrections to the velocities from Muraki et al. (1999) are given in (1). The $O(Ro)$ solutions include derivatives of the $O(1)$ solution, and in the point vortex case,

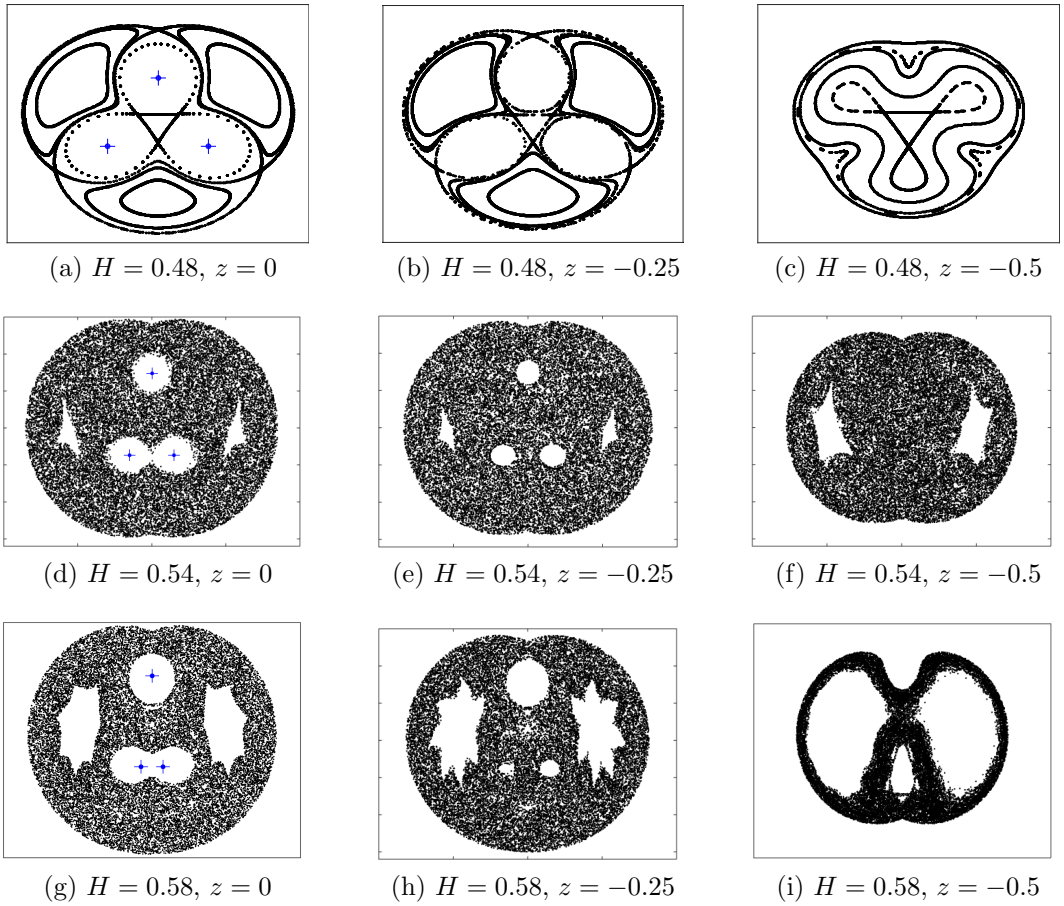

(a) $H = 0.48$, $z = 0$ (b) $H = 0.48$, $z = -0.25$ (c) $H = 0.48$, $z = -0.5$

(d) $H = 0.54$, $z = 0$ (e) $H = 0.54$, $z = -0.25$ (f) $H = 0.54$, $z = -0.5$

(g) $H = 0.58$, $z = 0$ (h) $H = 0.58$, $z = -0.25$ (i) $H = 0.58$, $z = -0.5$

Figure 1: Poincaré maps for SQG point vortices for three distinct vortex configurations sampled at three depths. Vortex positions are designated by blue crosses at the surface in (a,d,g). Compare the $z = 0$ plots (a,d,g) to solutions in Kuznetsov and Zaslavsky (1998).

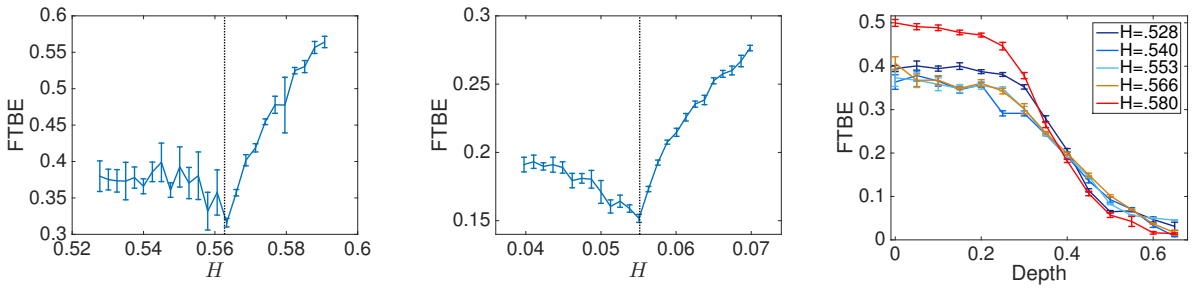

(a) SQG, $z = 0$ (b) 2D (c) SQG, select H

Figure 2: For three equal strength SQG vortices, the FTBE is calculated for various H, plotted (a) at the surface and (c) versus depth. For comparison, the FTBE for three equal strength two-dimensional vortices are shown in (b). Error bars of the FTBE are determined by statistical analysis of several choices of trajectory subsets. The vertical dotted line indicates the boundary between the two regimes of motion.

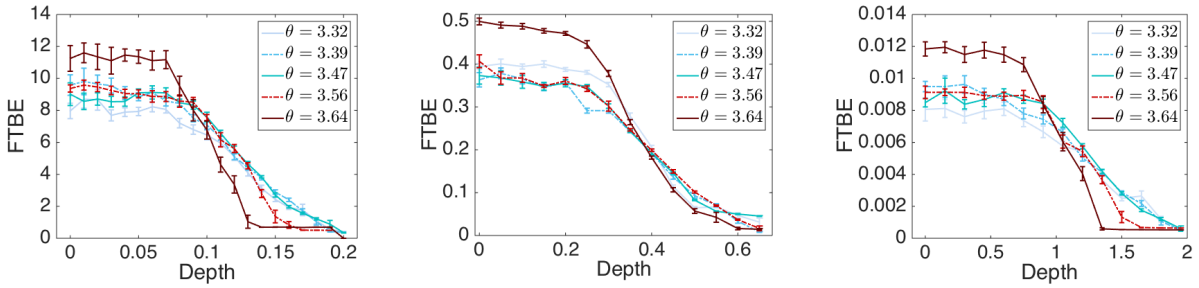

(a) $Ro = 0$, $L = 0.1$ (b) $Ro = 0$, $L = 1$ (c) $Ro = 0$, $L = 10$

Figure 3: Comparing the $O(1)$ equal strength point vortex solutions of FTBE vs. depth under changes to L. These plots show there is a critical depth beyond which the FTBE decreases sharply. For (b) $L = 1$ the critical depth appears to be $z = -0.25$, and increasing Ro increases the dropoff of FTBE for higher energies. For (a) $L = 0.1$, the critical depth has decreased to $z = -0.075$, and mixing has increased. For (c) $L = 10$, the critical depth has increased to $z = -0.75$, and mixing has decreased.

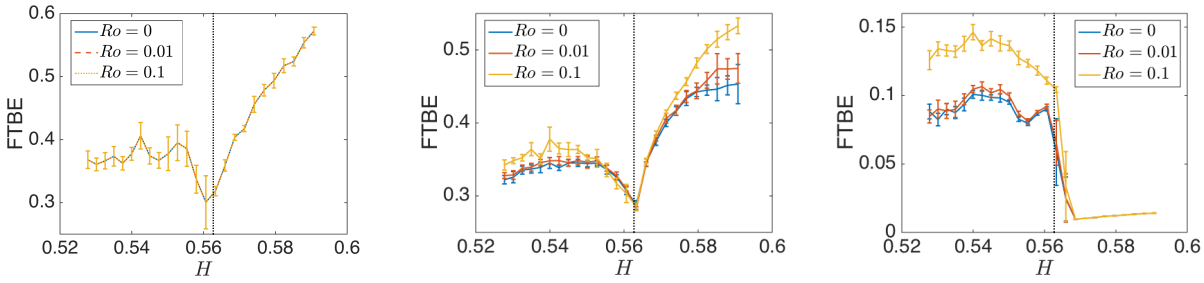

(a) $z = 0$ (b) $z = -0.25$ (c) $z = -0.5$

Figure 4: Comparison between the $O(1)$ equal strength point vortex solutions and those including w at height (a) $z = 0$, (b) -0.25, and (c) $z = -0.5$. Since $w = 0$ at the surface, it is expected that the solutions overlap as seen in (a).

where the $O(1)$ solution is singular, these terms are problematic. However, the vertical velocity can be obtained just from the energy conservation equation

$$\frac{D\theta}{Dt} + w = 0.$$

For the point vortex solution, it is found that

$$w = 3z \sum_j \frac{\kappa_j}{2\pi} \frac{(\mathbf{u} - \dot{\mathbf{x}}_j) \cdot (\mathbf{x} - \mathbf{x}_j)}{|\mathbf{x} - \mathbf{x}_j|^5} \tag{8}$$

where

$$\mathbf{u} - \dot{\mathbf{x}}_i = \sum_j{}' \frac{\kappa_j}{2\pi} \left[\frac{(-y + y_j, x - x_j, 0)}{|\mathbf{x} - \mathbf{x}_j|^3} - \frac{(-y_i + y_j, x_i - x_j, 0)}{|\mathbf{x}_i - \mathbf{x}_j|^3} \right]$$

and the prime on the sum indicates that the $i = j$ term is not considered. It is thus possible to examine the effect of vertical velocity on mixing, though in this case the solution is not dynamically consistent because the velocity is not divergenceless at $O(Ro)$.

FTBE results comparing the $O(Ro)$ and $O(1)$ solutions is shown in Figure 4 for $Ro = 0.01, 0.1$. At the surface, the solutions are identical, which follows from the constraint that $w = 0$ at the surface. At depths below the surface, including w seems to increase mixing, with larger w (resulting from larger Ro) producing more mixing. In the case with

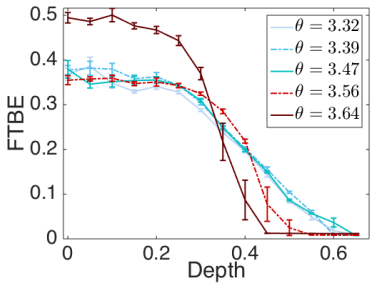

Figure 5: The FTBE vs. depth from the $O(Ro)$ equal strength point vortex solutions with $Ro = 0.01$. Compare to $O(1)$ in Figure 3(b). The dropoff appears steeper for higher energies.

w, the particle positions are projected into the x-y plane to obtain the maps. Here it appears that the area of the islands around each vortex increases with Ro, but the edge of the outer mixing boundary seems slightly larger in (c,d) for $Ro = 0.1$.

We can also examine how varying Ro as well as L affects the trend of FTBE with depth. There is no characteristic vertical length, but as seen in Figure 5(a,c,d), varying the characteristic horizontal length L will change the critical depth, from approximately $z = -0.075$ in the $L = 0.1$ case to approximately $z = -0.75$ for $L = 10$. We find that the critical depth seems to change according to $L^{1/2}$. The comparisons of Figure 5(a,c,d) additionally shows that the extent of mixing has decreased, which follows intuitively from the weaker velocities due to larger vortex spacing. As seen in Figure 5(b), changing Ro does not affect this critical depth, but does seem to cause a sharper dropoff in FTBE for higher energies. This may be due to an attraction towards periodic trajectories, so that particles below the critical depth tend to drift deeper and no longer experience mixing.

3 Elliptic Vortices

To examine a solution that is dynamically consistent at $O(Ro)$, a different model problem must be used. Harvey and Ambaum (2011) found that discontinuities in surface buoyancy necessarily result in infinite velocities at those locations. Thus, a continuous buoyancy distribution is needed. One such solution was detailed by Dritschel (2011), who considered the exact solution in QG for an ellipsoid containing a region of constant potential vorticity, which will rotate and maintain its shape (Dritschel et al., 2004). Dritschel orients this ellipsoid along the $z = 0$ plane so that one of its axes is vertical, then takes the limit as that axis length goes to zero. The potential vorticity is then contained on the boundary, and thus is an exact solution to SQG. The resulting governing equations are

$$\Delta\Phi^0 = 0\,, \qquad \left(\Phi^0_z\right)^s = \beta_m\sqrt{1 - \frac{x^2}{a^2} - \frac{y^2}{b^2}}, \tag{9}$$

where a, b are the semi-major and -minor axis lengths, respectively, aligned along the Cartesian axes, and β_m is a constant designating the strength of the ellipse.

A single elliptic vortex will rotate about its center and maintain its shape. Below the surface, three-dimensional trajectories in the flow are periodic. If multiple vortices are present, they will interact with one another and lose their elliptic shapes (Dritschel et al., 2004). Here we are not interested in solving this interaction exactly, but are looking for a manageable buoyancy solution that induces mixing in order to examine the effect

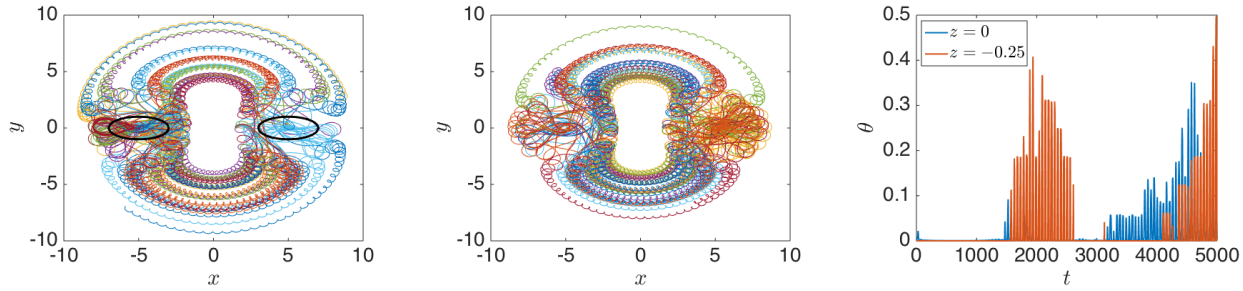

Figure 6: Trajectories for 16 particles initiated near (1.5,0) and integrated over a time interval of 5,000 on (a) $z = 0$ and (b) $z = -0.25$ in the frame of reference where the ellipse centroids remain on the x-axis. Initial ellipse positions are also shown in (a) in black. Additionally, (c) the mean buoyancy of the particles is shown for $z = 0$ (blue) and -0.25 (red) over time. Buoyancy results are nearly identical for $Ro = 0$, 0.01, 0.1.

of $O(Ro)$ velocities on transport. Hence the vortex interaction is approximated using a moment model following Bersanelli (2012) such that the ellipses will remain ellipses as the flow evolves.

For two identical elliptic vortices, there appears to be a negligible amount of mixing. The approximations lead to particle trajectories that intrude into the vortex, but the surrounding flow does not seem to exhibit chaos, as shown in Figure 6(a) in the frame of motion where the ellipses remain on the x-axis. These trajectories were computed for a time interval of 5,000, over which the ellipses completed 608 complete rotations about their centroids.

Trajectories are additionally examined away from the surface in Figure 6(b). These particles were initiated for the same x-y positions as in (a), but at a depth of $z = -0.25$. While qualitatively similar, these two sets of particles have distinct trajectories. The mean buoyancy of the particles is also shown in Figure 6(c), again showing the vertical dependence of the flow as well as that this approximation does not conserve buoyancy.

The results presented here are not meant to provide a rigorous proof that this flow does not result in chaos. Because we are looking for the effect of $O(Ro)$ velocities interacting with horizontal mixing, and not whether $O(Ro)$ velocities alone can induce mixing, the model flow should exhibit mixing at $O(1)$. Based on the mixing results for point vortices, three elliptic vortices are being considered in pending work. Both two and three ellipses, as well as the three point vortex solution, are further examined in Taylor (2016).

This work was funded by the *Ocean 3D+1* Office of Naval Research Multiple University Research Initiative.

References

Allshouse, M. R. and Peacock, T. (2015). Lagrangian based methods for coherent structure detection. *Chaos*, 25:097617.

Aref, H. and Pomphrey, N. (1980). Integrable and chaotic motions of four vortices. *Phys. Lett.*, 78A:297–300.

Bersanelli, M. (2012). Moment model for the dynamics of a pair of quasi-geostrophic vortices. *MS Thesis. Università degli Studi di Milano.*

Bowen, R. (1973). Topological entropy for noncompact sets. *Trans. Amer. Math. Soc.*, 184:125–136.

Budišić, M. and Thiffeault, J.-L. (2015). Finite-time braiding exponents. *Chaos*, 25:087407.

Dritschel, D. G. (2011). An exact steadily rotating surface quasi-geostrophic elliptical vortex. *Geophys. Astrophys. Fluid Dyn.*, 105:368–376.

Dritschel, D. G., Reinaud, J. N., and McKiver, W. J. (2004). The quasi-geostrophic ellipsoidal vortex model. *J. Fluid. Mech.*, 505:201–223.

Harvey, B. J. and Ambaum, M. H. P. (2011). Perturbed Rankine vortices in surface quasi-geostrophic dynamics. *Geophys. Astrophys. Fluid Dyn.*, 105:377–391.

Held, I. M., Pierrehumbert, R. T., Garner, S. T., and Swanson, K. L. (1995). Surface quasi-geostrophic dynamics. *J. Fluid Mech.*, 282:1–20.

Kuznetsov, L. and Zaslavsky, G. M. (1998). Regular and chaotic advection in the flow field of a three-vortex system. *Phys. Rev. E*, 58:7330–7349.

Muraki, D. J., Snyder, C., and Rotunno, R. (1999). The next-order corrections to quasi-geostrophic theory. *J. Atmos. Sci.*, 56:1547–1560.

Newhouse, S. and Pignataro, T. (1993). On the estimation of topological entropy. *J. Stat. Phys.*, 72:1331–1351.

Peacock, T. and Dabiri, J. (2010). Introduction to focus issue: Lagrangian Coherent Structures. *Chaos*, 20(017501).

Taylor, C. K. (2016). Surface quasi-geostrophic vortex dynamics and resulting transport with weak vertical motion. *PhD. University of California, San Diego.*

Thiffeault, J.-L. and Budišić, M. (2014). *Braidlab: A software package for braids and loops.* e-print arXiv:1410.0849. Retrieved February 2015.

Vallis, G. K. (2006). *Atmospheric and Oceanic Fluid Dynamics.* Cambridge University Press.